ARTICLE IN PRESS

Available online at www.sciencedirect.com

SCIENCE DIRECT®

ELSEVIER

International Journal of Rock Mechanics & Mining Sciences ▮ (▮▮▮▮) ▮▮▮–▮▮▮

International Journal of Rock Mechanics and Mining Sciences

www.elsevier.com/locate/ijrmms

Transverse drilling-induced tensile fractures in the West Tuna area, Gippsland Basin, Australia: implications for the in situ stress regime

E.J. Nelson[a,*], J.J. Meyer[b], R.R. Hillis[a], S.D. Mildren[b]

[a]*Australian School of Petroleum, The University of Adelaide, Santos Petroleum Engineering Building, South Australia, Australia*
[b]*JRS Petroleum Research, Adelaide, Australia*

Accepted 9 December 2004

Abstract

Drilling-induced tensile fractures (DITFs) have been interpreted on image logs from vertical wells in the Gippsland Basin, offshore southeastern Australia. Interpreted axial (vertical) DITFs have previously been well described worldwide. We also interpret transverse (horizontal) DITFs, which are horizontal fractures that are electrically conductive, non-planar, bimodal and constrained to the tensile region of the wellbore.

Elasticity theory predicts formation of both transverse and axial drilling-induced tensile fractures (DITFs) in vertical wells depending on the magnitude of the principal in situ stresses, pore-pressure and mudweight. Drilling-induced tensile fractures initiate in very specific stress environments. Axial DITFs can closely constrain a lower bound to the maximum horizontal stress ($S_{H\,max}$) magnitude where the minimum horizontal ($S_{h\,min}$) stress is known. If transverse DITFs are observed, they can constrain a lower bound to maximum and minimum horizontal stress magnitudes. The observation of transverse DITFs on image logs can constrain the stress field to one on the border of strike-slip and reverse faulting ($S_{H\,max} \gg S_{h\,min} \sim S_v$) without requiring knowledge of the $S_{h\,min}$ or $S_{H\,max}$ magnitude. The observation of transverse DITFs in the West Tuna area combined with wireline log data, leak-off tests and pore pressure data are used to constrain the in situ stress tensor. The interpreted in situ stress tensor lies on the border of a strike-slip and reverse faulting regime ($S_{H\,max} \sim 40.5$ MPa/km $> S_{h\,min} \approx S_v \sim 21$ MPa/km). Interpreted data from leak-off tests in the West Tuna area confirm that $S_{h\,min} \sim S_v$.

Keywords: Drilling induced tensile fractures; In situ stress; Gippsland Basin

1. Introduction

Accurate knowledge of the in situ stress tensor is critical to the efficient development of petroleum provinces, mineral resources and underground excavations. The in situ stress tensor has applications to petroleum and geothermal well design including the assessment of wellbore stability and the design of fracture stimulation and waterflooding programs. Similarly, knowledge of the in situ stress tensor is critical to civil and mining engineering problems such as stability of underground excavations (tunnels, mines, shafts, stopes), disposal of radioactive waste, drilling and blasting, and design of support structures. The magnitude of the maximum horizontal stress ($S_{H\,max}$) is commonly the most difficult aspect of the in situ stress tensor to constrain [1]. It can be determined where breakouts or drilling-induced tensile fractures (DITFs) are observed on image logs and where rock strength is known [2,3]. Occurrences of DITFs that propagate axially or are inclined to a vertical wellbore have been well documented and are used routinely to constrain $S_{H\,max}$ [3–8].

Analysis of image logs from two wells in the West Tuna area of the Gippsland Basin revealed fractures

*Corresponding author. Tel.: +61 8 8303 4308; fax: +61 8 8303 4345.
E-mail address: enelson@asp.adelaide.edu.au (E.J. Nelson).

1365-1609/$ - see front matter © 2005 Elsevier Ltd. All rights reserved.
doi:10.1016/j.ijrmms.2004.12.001

that were approximately horizontal (transverse to the wellbore axis) in orientation, non-planar and restricted in occurrence to the tensile region of the wellbore. The character and morphology of the fractures suggest that they may be drilling-induced, stress-related features rather than horizontal natural fractures.

The TDITFs presented herein are very similar to horizontal fractures described by Morin and Flamand [9] in image logs from the eastern equatorial Pacific. However, these authors describe the fractures as being induced by thermal stresses due to circulation of cold seawater against hot rocks. We believe that the TDITFs in West Tuna form in response to stress perturbation at the wellbore wall caused by high horizontal stresses in West Tuna. Elasticity theory is used herein to show that DITFs can form axially or transversely to a vertical well, depending on the in situ stress regime, rock strength and mudweight. Furthermore, we verify using an independently derived in situ stress tensor that where transverse DITFs are interpreted, close constraints can be placed on the magnitudes of the maximum and minimum horizontal stresses.

1.1. Stresses around a vertical wellbore

Drilling-induced tensile fractures form as a consequence of the stress concentration about the wellbore generated during drilling [10]. As the well is drilled, the wellbore wall must support stresses previously carried by the removed rock. This causes stress concentration about the borehole that depends on the orientations of the wellbore and the far field in situ stress tensor [11–13].

Assuming that the vertical stress is a principal stress, then three principal stresses act about the wall of a vertical well (Fig. 1). These are:

1. the effective radial stress (σ_{rr}) which acts normal to the wellbore;
2. the effective axial stress (σ_{zz}) which acts parallel to the wellbore axis, and;
3. the effective circumferential stress ($\sigma_{\theta\theta}$), which acts orthogonal to σ_{rr} and σ_{zz}.

The near wellbore stresses in impermeable, elastic, homogeneous and isotropic rock are defined by the Kirsch [13] equations. Although the Kirsch equations are simplistic, they are considered to adequately represent the near wellbore stress environment in most regions [1,3,7]. Since petroleum wells are typically drilled overbalanced and mud cake forms at the wellbore wall, the approximation of impermeability is also generally considered valid for reservoir rocks.

The magnitude of the near wellbore stresses depends on the magnitude of the far field effective stresses ($S'_{\mathrm{H\ max}}$, $S'_{\mathrm{h\ min}}$ and S'_{v}), the radius of the wellbore (R), distance from the wellbore (r) and the pore pressure

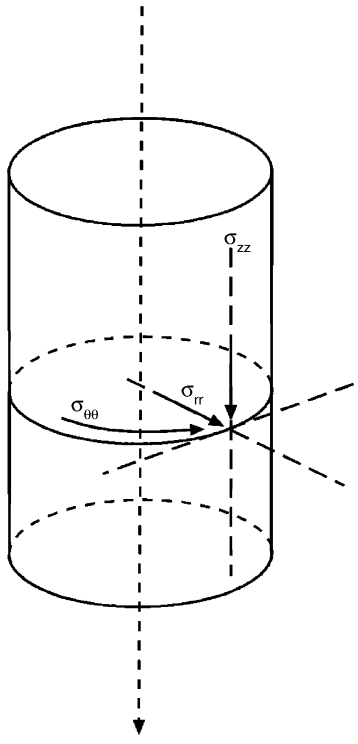

Fig. 1. Vertical wellbore showing orientations of the circumferential ($\sigma_{\theta\theta}$), axial (σ_{zz}) and radial (σ_{rr}) stresses.

(P_{p}). The Kirsch equations are expressed as

$$\sigma_{\theta\theta} = \frac{1}{2}(S'_{\mathrm{H\ max}} + S'_{\mathrm{h\ min}})\left(1 + \frac{R^2}{r^2}\right) - \frac{1}{2}(S'_{\mathrm{H\ max}} + S'_{\mathrm{h\ min}})\left(1 + 3\frac{R^4}{r^4}\right)\cos 2\theta - \frac{\Delta P R^2}{r^2}, \quad (1)$$

$$\sigma_{rr} = \frac{1}{2}(S'_{\mathrm{H\ max}} + S'_{\mathrm{h\ min}})\left(1 - \frac{R^2}{r^2}\right) + \frac{1}{2}(S'_{\mathrm{H\ max}} - S'_{\mathrm{h\ min}})\left(1 - 4\frac{R^2}{r^2} + 3\frac{R^4}{r^4}\right)\cos 2\theta + \frac{\Delta P R^2}{r^2}, \quad (2)$$

$$\tau_{r\theta} = \frac{1}{2}(S'_{\mathrm{H\ max}} + S'_{\mathrm{h\ min}})\left(1 + 2\frac{R^2}{r^2} - 3\frac{R^4}{r^4}\right)\sin 2\theta, \quad (3)$$

$$\sigma_{zz} = S'_{\mathrm{v}} - 2\nu(S'_{\mathrm{H\ max}} - S'_{\mathrm{h\ min}})\cos 2\theta - P_{\mathrm{p}}, \quad (4)$$

where $\tau_{r\theta}$ is the tangential shear stress, ν is Poisson's ratio, ΔP is the difference between mud pressure and pore pressure ($P_{\mathrm{w}} - P_{\mathrm{p}}$), and θ is the angle between the $S_{\mathrm{H\,max}}$ azimuth and north (Fig. 2).

If stresses at the wellbore wall are considered (i.e. where $R = r$), the Kirsch equations may be simplified as

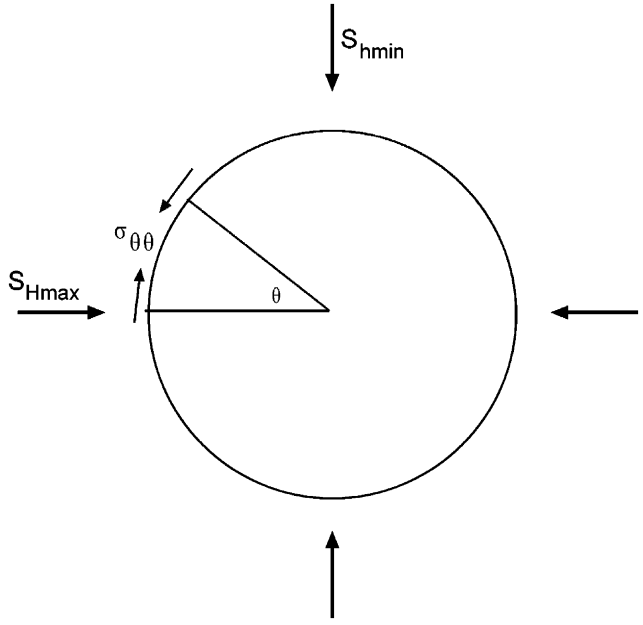

Fig. 2. Cross-section of a wellbore showing that position around the wellbore (relative bearing) is described by the angle (θ) measured clockwise from $S_{H\,max}$.

follows [14]:

$$\sigma_{\theta\theta} = (S'_{H\,max} + S'_{h\,min}) - 2(S'_{H\,max} - S'_{h\,min}) \times \cos 2\theta - \Delta P, \quad (5)$$

$$\sigma_{rr} = \Delta P, \quad (6)$$

$$\sigma_{zz} = S'_{v} - 2\nu(S'_{H\,max} - S'_{h\,min})\cos 2\theta - P_{p}, \quad (7)$$

$$\tau_{r\theta} = 0. \quad (8)$$

The above equations are written in terms of the effective far field principal stresses. Eqs. (5)–(8) can be expressed in terms of total stresses as follows:

$$\sigma_{\theta\theta} = (S_{H\,max} + S_{h\,min}) - 2(S_{H\,max} - S_{h\,min}) \times \cos 2\theta - P_{w} - P_{p}, \quad (9)$$

$$\sigma_{rr} = \Delta P, \quad (10)$$

$$\sigma_{zz} = S_{v} - 2\nu(S_{H\,max} + S_{h\,min})\cos 2\theta - P_{p}, \quad (11)$$

$$\tau_{r\theta} = 0. \quad (12)$$

$S_{H\,max}$, $S_{h\,min}$ and S_{v} represent the maximum horizontal, minimum horizontal and vertical stress magnitudes. P_{w} is the wellbore fluid pressure (mudweight).

If the circumferential stress and axial stress are plotted with respect to position around the wellbore wall (Fig. 3) it can be shown that $\sigma_{\theta\theta}$, and σ_{zz} are maximum when θ is equal to 90° (i.e. at the azimuth of far-field $S_{h\,min}$), and minimum when θ is equal to 0° (i.e. at the azimuth of far-field $S_{H\,max}$). Eq. (9) can be simplified for the conditions where $\theta = 0°$ and $\theta = 90°$.

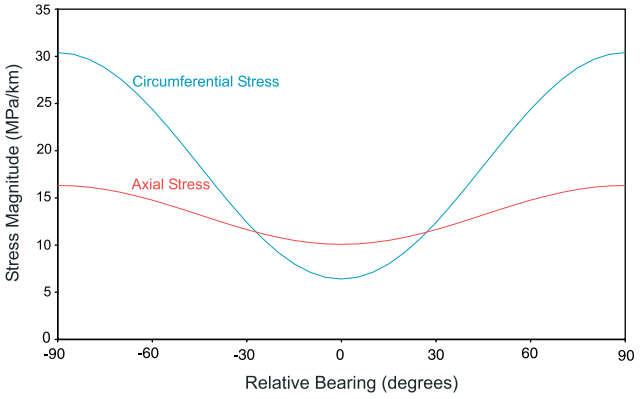

Fig. 3. Example wellbore stress diagram showing the axial stress (σ_{zz}) and the circumferential stress ($\sigma_{\theta\theta}$) as a function of relative bearing around the wellbore.

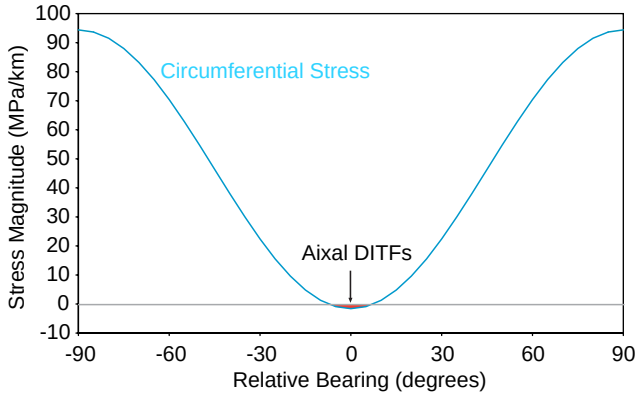

Fig. 4. Wellbore stresses diagram showing the criterion required to form axial DITFs ($\sigma_{\theta\theta} \leqslant 0$).

$$\sigma_{\theta\theta\,max} = 3S_{H\,max} - S_{h\,min} - P_{w} - P_{p}. \quad (13)$$

$$\sigma_{\theta\theta\,min} = 3S_{h\,min} - S_{H\,max} - P_{w} - P_{p}. \quad (14)$$

The Kirsch [13] equations can also be applied to inclined boreholes as discussed in Peska and Zoback [4].

1.2. Axial drilling-induced tensile fractures

Tensile failure occurs when the minimum circumferential stress around the wellbore is less than the tensile strength of the rock [4,7] (Fig. 4). The circumferential stress is minimised at $\theta = 0$, hence DITFs form in the wellbore at the azimuth of $S_{H\,max}$. Therefore, Eq. (14) can be modified to represent the criterion for formation of axial DITFs in elastic, impermeable rocks in vertical wellbores such that:

$$\sigma_{\theta\theta\,min} = 3S_{h\,min} - S_{H\,max} - P_{w} - P_{p} \leqslant T. \quad (15)$$

where T is the tensile rock strength. The tensile rock strength is often assumed to be negligible hence, axial DITFs tend to occur when $\sigma_{\theta\theta\,\mathrm{min}}$ is less than zero and Eq. (15) becomes [3]:

$$\sigma_{\theta\theta\,\mathrm{min}} = 3S_{\mathrm{h\,min}} - S_{\mathrm{H\,max}} - P_{\mathrm{w}} - P_{\mathrm{p}} \leqslant 0. \quad (16)$$

Drilling-induced tensile fractures initiate in deviated wellbores when the minimum effective stress tangential to the wellbore is less than the tensile strength of the rock. This means that DITFs in deviated wells form at an angle between the maximum effective stress tangential to the wellbore and the borehole axis. These DITFs are normally referred to as inclined [4]. For a discussion of stresses in elastic impermeable rock around arbitrarily inclined boreholes see Haimson and Fairhurst [15] and Peska and Zoback [4].

1.3. Transverse drilling-induced tensile fractures

Transverse DITFs initiate in a more tightly constrained near wellbore stress environment than axial DITFs. Assuming elastic impermeable rocks, two criteria must be met to facilitate formation of transverse DITFs (Fig. 5).

1. The axial wellbore stress must be less than or equal to zero ($\sigma_{zz} \leqslant 0$) permitting the development of horizontal fractures.
2. The axial wellbore stress must be less than or equal to the circumferential stress ($\sigma_{zz} \leqslant \sigma_{\theta\theta}$) precluding the formation of vertical DITFs (assuming vertical DITFs do not co-exist with the transverse DITFs).

As with the circumferential stress, the axial stress around the wellbore is minimised when $\theta = 0$. Consequently Eq. (11) can be rewritten as

$$\sigma_{zz\,\mathrm{min}} = S_{\mathrm{v}} - 2\nu(S_{\mathrm{H\,max}} - S_{\mathrm{h\,min}}) - P_{\mathrm{p}}. \quad (17)$$

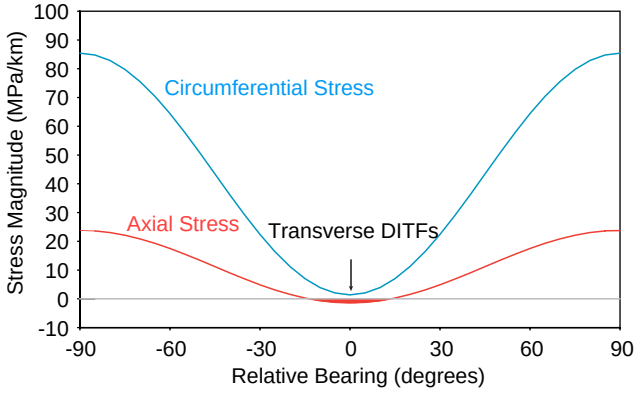

Fig. 5. Wellbore stresses diagram showing the criterion required to form transverse DITFs (the axial stress is less than zero and less than the circumferential stress).

Assuming horizontal DITFs occur where $\sigma_{zz\,\mathrm{min}} \leqslant 0$ and $\sigma_{zz\,\mathrm{min}} \leqslant \sigma_{\theta\theta\,\mathrm{min}}$, Eq. (17) can be rewritten as

$$S_{\mathrm{v}} - 2\nu(S_{\mathrm{H\,max}} - S_{\mathrm{h\,min}}) - P_{\mathrm{p}} \leqslant 0 \quad (18)$$

and combined with Eq. (14) to give

$$S_{\mathrm{v}} - 2\nu(S_{\mathrm{H\,max}} - S_{\mathrm{h\,min}}) - P_{\mathrm{p}} \leqslant 3S_{\mathrm{h\,min}} - S_{\mathrm{H\,max}} - P_{\mathrm{w}} - P_{\mathrm{p}}. \quad (19)$$

Eq. (19) may be simplified further to give

$$S_{\mathrm{v}} + S_{\mathrm{h\,min}} + (2\nu - 3) + S_{\mathrm{H\,max}}(1 - 2\nu) + P_{\mathrm{w}} \leqslant 0. \quad (20)$$

Eqs. (18) and (20) can be used to determine the upper and lower bounds to $S_{\mathrm{H\,max}}$ where transverse DITFs are observed on image logs in vertical wells and where S_{v}, $S_{\mathrm{h\,min}}$, P_{w} and ν can be determined from wireline log data and rock strength testing. These equations will be revisited subsequently, however brief examination of Eq. (18) shows that if S_{v} is ~22.6 MPa/km (1 psi/ft) and P_{p} is hydrostatic then the differential horizontal stress must be high ($S_{\mathrm{H\,max}}$ magnitude must be ~twice $S_{\mathrm{h\,min}}$) to facilitate the formation of transverse DITFs. Similarly, examination of Eq. (20) suggests that $S_{\mathrm{h\,min}}$ must be high (approximately S_{v}) to facilitate formation of transverse DITFs. Eqs. (18) and (20) suggest that transverse drilling-induced fracturing can only occur in stress states between strike-slip and reverse faulting.

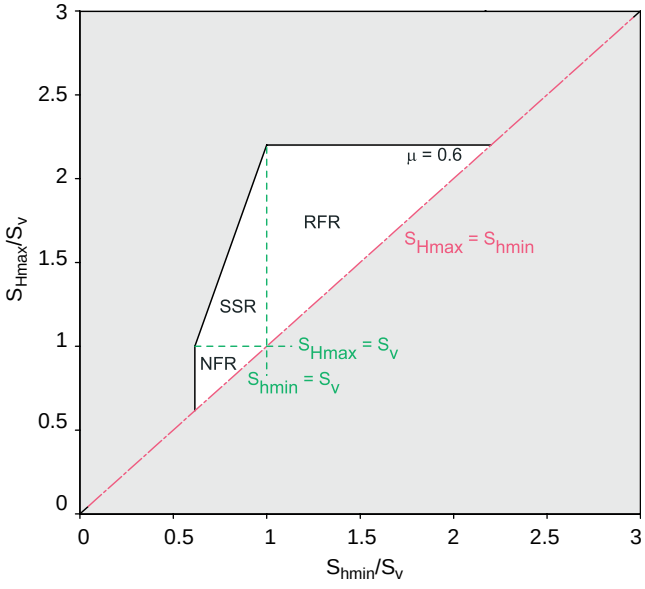

Fig. 6. Allowable region diagram. The white region represents stress magnitudes within frictional limits. RFR refers to a reverse fault stress regime. SSR refers to a strike-slip fault stress regime. NFR refers to a normal fault stress regime. The figure assumes a μ of 0.6 and hydrostatic pore pressure.

1.4. Allowable region diagrams

The range of possible relative principal stress magnitudes for normal, strike-slip and reverse faulting environments can be visualised on an allowable region diagram [1,14] (Fig. 6). The allowable stress conditions for a particular geographic region are assumed to lie within an area defined by frictional limits (Fig. 6). Frictional limits theory states that the magnitude of $S_{\mathrm{H\,max}}$ can be constrained in strike-slip and reverse faulting environments by assuming that the ratio of the maximum to minimum effective stress cannot exceed the magnitude required to cause faulting on an optimally oriented pre-existing fault [16]. The frictional limit to stress is given by

$$\frac{S_1 - P_p}{S_3 - P_p} \leqslant \{\sqrt{(\mu^2 + 1)} + \mu\}^2, \tag{21}$$

where μ is the coefficient of friction on an optimally oriented pre-existing fault, S_1 is the maximum principal stress and S_3 is the minimum principal stress [12]. The above equation effectively states that if the ratio of $S_1 - P_p / S_3 - P_p$ exceeds μ then slip will occur, hence frictional limits provide an upper bound to $S_{\mathrm{H\,max}}$ where it is the maximum principal stress. Considering that 0.6–0.8 are common values for μ [17], then by substitution into Eq. (21) the ratio of maximum to minimum effective stress generally falls between 3.12 and 4.33.

Frictional limits constrain the allowable values of $S_{\mathrm{H\,max}}$ to within the black outline in Fig. 6 (where $\mu = 0.6$). The criterion $S_{\mathrm{H\,max}} \geqslant S_{\mathrm{h\,min}}$ further constrains the possible stress states to the upper left of the pink line, and hence to the yellow area in Fig. 6. The green lines representing $S_{H\ \mathrm{max}} = S_v$ and $S_{h\ \mathrm{min}} = S_v$ separate the normal, strike-slip and reverse fault regimes (Fig. 6) as defined by Anderson [18].

Eqs. (18) and (20) can be plotted as lines on the allowable region diagram facilitating determination of the stress region in which transverse DITFs may form (Fig. 7). Considering the criterion $\sigma_{\theta\theta} = \sigma_{zz}$ (Eq. (20)) and a generalised in situ stress tensor where S_v ~22.6 MPa/km (1 psi/ft), $v \sim 0.26$, P_p~9.8 MPa/km and P_w~9.8 MPa/km, then allowable values for $S_{\mathrm{H\,max}}$ must lie in the region to the right of the solid line labelled $S_{qq} = S_{zz}$ in Fig. 7. Similarly the criterion $\sigma_{zz} = 0$ (Eq. (18)) constrains the allowable values of $S_{\mathrm{H\,max}}$ to the left of the solid line labelled $S_{zz} = 0$ in Fig. 7. The observation of transverse DITFs on image logs can therefore constrain the stress field to one on the border of strike-slip and reverse faulting ($S_{\mathrm{H\ max}} \geqslant S_{\mathrm{h\ min}} \sim S_v$), without requiring knowledge of the $S_{\mathrm{h\,min}}$ or $S_{\mathrm{H\,max}}$ magnitude.

The occurrence of transverse DITFs in a particular stress regime is strongly influenced by rock properties. Poisson's ratio is an important parameter in Eq. (18) and (20), which determines the slope and position of the lines in the allowable stress region. The co-efficient of friction is also important, determining the frictional limits boundary and hence the upper limit to $S_{\mathrm{H\,max}}$.

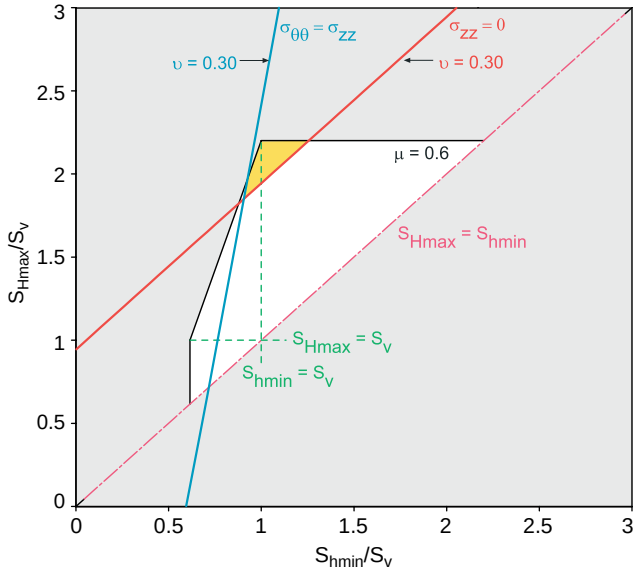

Fig. 7. Allowable region diagram. The solid lines represent the criteria $\sigma_{\theta\theta} = \sigma_{zz}$ (Eq. (20)) and $\sigma_{zz} = 0$ (Eq. (18)), respectively. The shaded region represents the possible stress regimes assuming transverse DITFs are observed. The figure assumes a μ of 0.6, $S_v = 22.6$ MPa/km and hydrostatic, in balance drilling conditions.

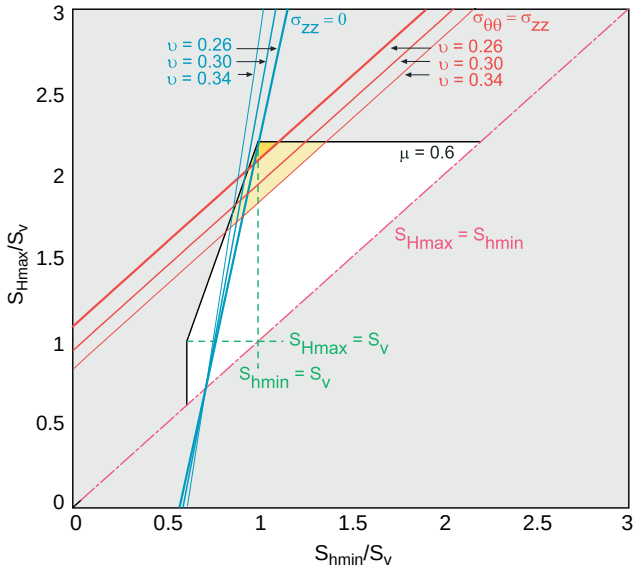

Fig. 8. Allowable region diagram. The solid lines represent the criteria $\sigma_{\theta\theta} = \sigma_{zz}$ (Eq. (20)) and $\sigma_{zz} = 0$ (Eq. (18)). The shaded region represents the possible stress regimes assuming transverse DITFs are observed and Poissons ratios of 0.26 (thick lines), 0.30 (intermediate lines) and 0.34 (thin lines). The figure assumes a μ of 0.6, $S_v = 22.6$ MPa/km and hydrostatic, in balance drilling conditions.

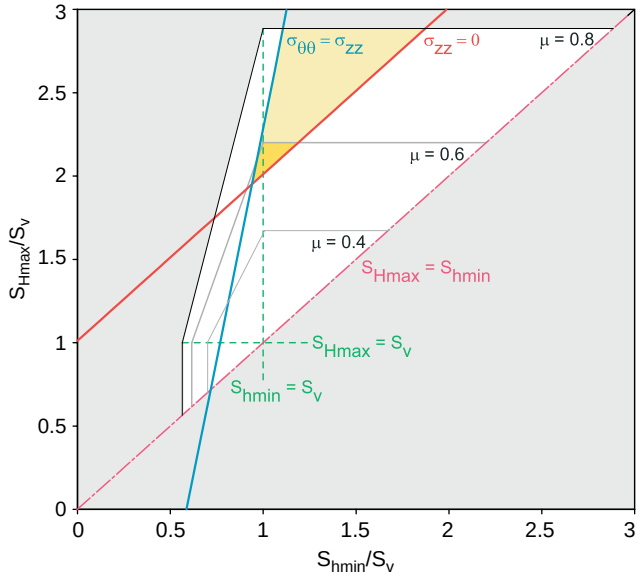

Fig. 9. Allowable region diagram. The solid lines represent the criteria $\sigma_{\theta\theta} = \sigma_{zz}$ (Eq. (20)) and $\sigma_{zz} = 0$ (Eq. (18)). The shaded region represents the possible stress regimes assuming transverse DITFs are observed, $v = 0.28$, $S_v = 22.6$ MPa/km and hydrostatic, in balance drilling conditions. The upper boundaries to $S_{H\,max}$ have been determined for a μ of 0.4, 0.6 and 0.8.

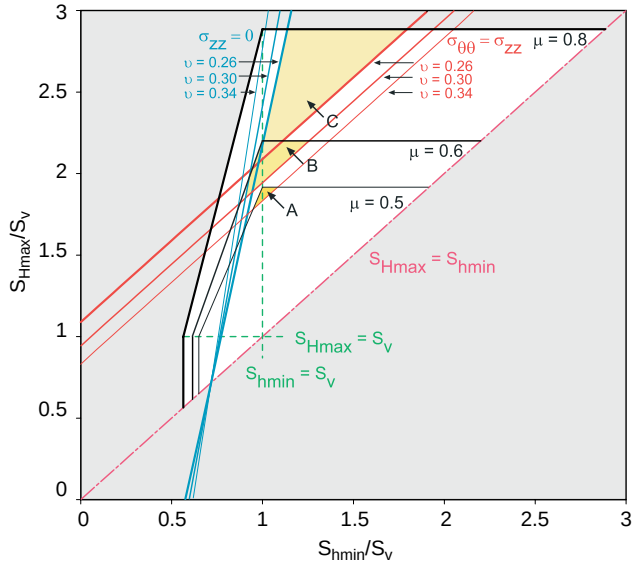

Fig. 10. Allowable region diagram. The solid lines represent the criteria $\sigma_{\theta\theta} = \sigma_{zz}$ (Eq. (20)) and $\sigma_{zz} = 0$ (Eq. (18)). The shaded regions represent the possible stress regimes assuming transverse DITFs are observed and three hypothetical rock types. A stress state where $S_v = 22.6$ MPa/km, pore pressure is hydrostatic, and the well is in balance.

Eq. (18) and (20) have been plotted on an allowable region diagram to illustrate the effect of Poisson's ratio on the formation of transverse DITFs (Fig. 8). Fig. 8 illustrates that as Poisson's ratio increases, the stress region in which transverse DITFs may form broadens. This is also true as μ increases (Fig. 9). The reliability of the in situ stress tensor determination from the observation of DITFs is therefore dependent on how accurately rock properties are known. For example, the presence of DITFs in a shaly sand (where $S_v = 22.6$, $P_p = 9.8$, $P_w = 9.8$, $v = 0.3$ and $\mu = 0.6$), constrains the stress states to region B in Fig. 10. If the transverse DITFs are observed in a shale ($v = 0.34$, $\mu = 0.5$) or hard sandstone ($v = 0.26$, $\mu = 0.8$) then the stress regime could be constrained to regions A and C, respectively.

2. Interpreting drilling-induced tensile fractures on image logs

It is often difficult to distinguish DITFs on image logs from post-depositional features such as natural fractures and faults and syn-depositional features such as bedding. This was found to be the case when analysing images from the West Tuna area where bedding, natural fractures and DITFs are characterised by shallow dip.

Generally two types of DITFs are reported in the literature as being observed on image logs [3].

1. Pairs of fractures, discontinuous around the borehole, but parallel to the borehole axis and offset by 180° (Fig. 11). These are axial DITFs and reflect that the wellbore axis is parallel to a principal stress axis (S_v).
2. Fracture traces offset by 180° at the borehole wall but inclined with respect to the borehole axis. They are often referred to as inclined or *en echelon* fracture traces (Fig. 11). These are also axial DITFs, but in this case the wellbore axis is inclined with respect to a principal stress axis (S_v).

The mathematical criterion for the formation of axial DITFs in the wellbore determines the criterion for their interpretation (Eq. (16)). Assuming elastic conditions then axial DITFs must be [3,19]:

- axial to the wellbore;
- electrically conductive (open and mud-filled in the near wellbore);
- discrete and confined to the tensile region of the wellbore, and;
- non-planar.

Where inclined DITFs are chiral (i.e. they exhibit 'handedness') they can also be confidently distinguished from natural fractures.

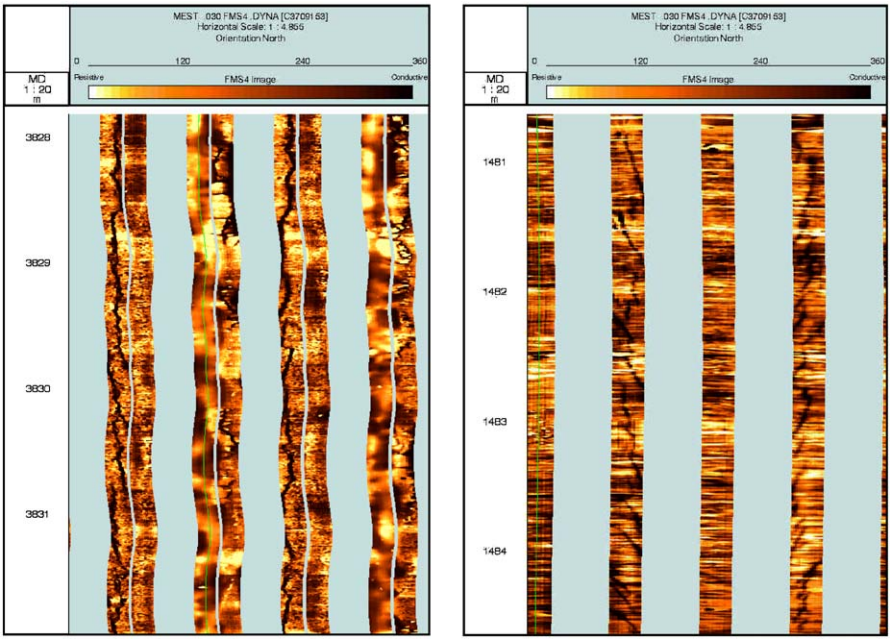

Fig. 11. Image logs showing axial and inclined DITFs (depth scale is in metres, the image extends from 0 to 360° around the wellbore). The dark colour of the fractures indicates that they are electrically conductive. Left: axial DITFs forming on opposing pads at 90° to the breakouts. Right: inclined DITFs forming on orthogonal pads.

2.1. Transverse drilling-induced tensile fractures

As with axial DITFs, the formation of transverse DITFs is a function of in situ stress, rock strength and mudweight. Therefore the proposed criteria for formation and interpretation of transverse DITFs on image logs are similar to those for axial DITFs and are based on the criteria above. Transverse DITFs must be:

- transverse across the wellbore;
- electrically conductive;
- discrete and confined to the tensile region of the wellbore;
- non-planar (they show small kinks and are not perfectly straight); and
- discordant to bedding.

These rules are used to distinguish transverse DITFs from near horizontal natural fractures that are also observed on the West Tuna image logs.

3. Drilling-induced tensile fracture occurrence in West Tuna

Transverse fractures believed to be drilling-induced were observed in image logs from the West Tuna_8 and West Tuna_39 wells (Table 1). Both West Tuna_8 and West Tuna_39 are near vertical at the depth of the fractures (Table 1). The observed fractures are transverse to the wellbore (at the azimuth of $S_{H\,max}$), and are electrically conductive suggesting that they are open and accepting drilling fluid. The fractures are restricted in occurrence to the tensile region of the wellbore, indicating that they have formed in response to the near wellbore stress environment. The fractures are discrete and non-planar particularly as the fracture propagates from the $S_{H\,max}$ azimuth. This further suggests that the interpreted fractures are drilling-induced (Fig. 12). To ensure that the fractures are not bedding related, the bedding immediately above and below the fractures was interpreted and found to be of similar dip but of different azimuth to the DITFs (Fig. 13). The non-planar and irregular nature of the fracture plane also suggests that they are not open natural fractures.

3.1. Previous interpretations of transverse drilling-induced tensile fractures

Transverse tensile fractures have been observed in image logs from the eastern equatorial Pacific Ocean [9]. These fractures were restricted to the tensile parts of the wellbore wall and were located at the upper and lower boundaries of borehole breakouts [9]. Morin and Flamond [9] noted that the interpreted tensile fractures formed in zones in the wellbore where drilling-mud had been circulated. They showed that the failure could be attributed ephemeral thermal stresses induced by the repeated injection and circulation of cold seawater

Table 1
Depths of observed DITFs from image logs and well orientation at depth of DITF occurrence

Well	DITF Type	TVDSS (m)	Hole Azi (°)	Hole Devi (°)
West Tuna_w39	Transverse	2672–2686	045	2
West Tuna_w08	Transverse	3191–3194	311	4.2

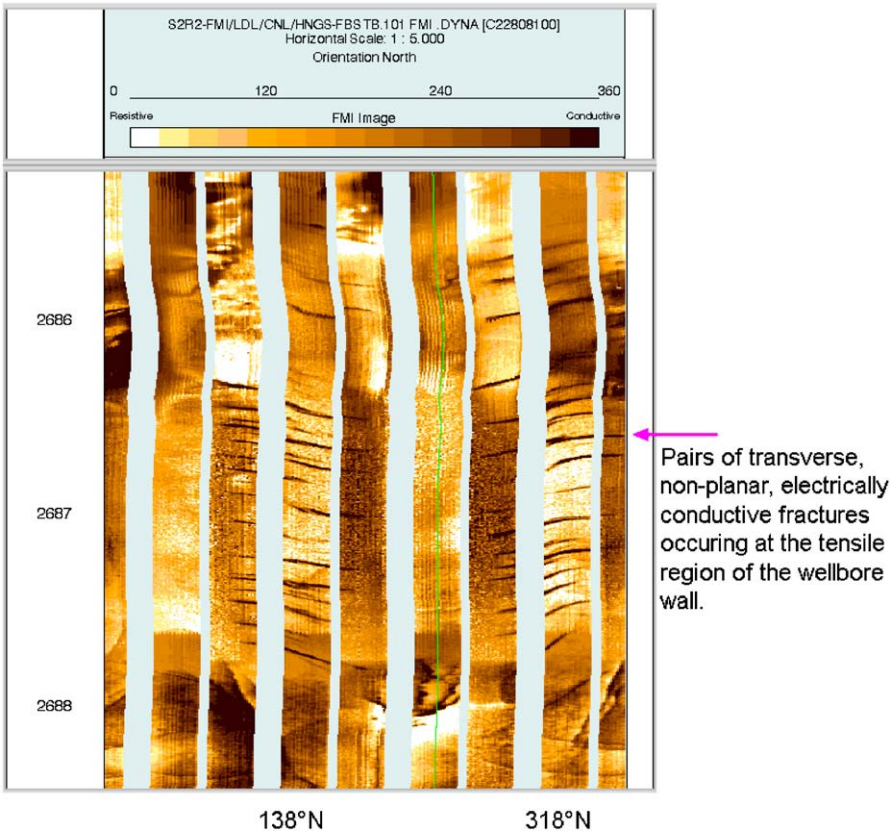

Fig. 12. Transverse DITFs interpreted on an image log from the West Tuna_39 well. The fractures are electrically conductive, transverse (at the azimuth of $S_{H\,max}$), restricted to the tensile region of the wellbore and non-planar.

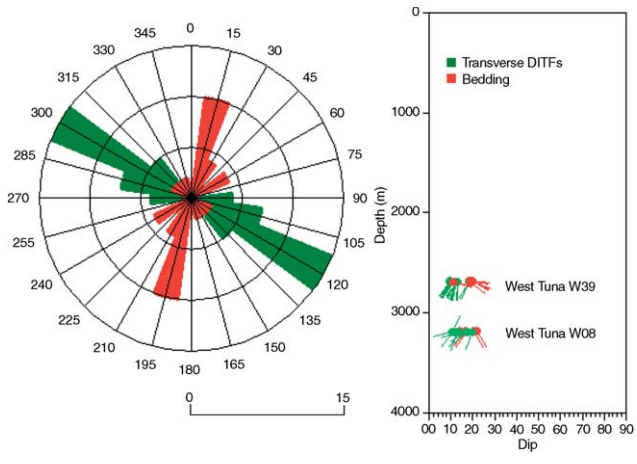

Fig. 13. Left: stereonet illustrating the azimuthal difference between the transverse DITFs and bedding planes in West Tuna_8 and West Tuna_39. Right: dip tadpoles.

against hot rock. Thermally induced stresses have also previously been shown to produce axial (shear and tensile) wellbore failure [3,20]. There is no evidence for significant thermal perturbation due to drilling in West Tuna. However as discussed above, the authors believe that transverse DITFs may form (where there is no thermal stress perturbation) in specific stress regimes on the border of strike-slip and reverse faulting.

4. West Tuna in situ stress tensor

Although the transverse fractures observed in the West Tuna image logs fit the criteria devised for interpretation of transverse DITFs, further justification for their interpretation comes from additional analysis of the in situ stress tensor. Determining the in situ stress tensor from drilling and wireline-log data is now routine

and is not discussed comprehensively herein. The reader is directed to:

- Prensky [21], Bell [22,23] and references therein for an overview of using wellbore failure to determine the $S_{H\,max}$ orientation,
- Tingay et al. [24] and references therein for a discussion of determining the vertical stress from density, sonic and check shot data,
- Breckels and van Eekelen [25] and Aadnoy [26] for a discussion of using the lower bound to leak-off to estimate $S_{h\,min}$, and
- Zimmerman et al. [27] and Goode et al. [28] for a discussion of determining reservoir pressure from the MDT tool.

Ninety-one borehole breakouts, and two sets of transverse DITFs were observed in image logs from six wells located in the West Tuna area of the Gippsland Basin. The breakouts indicate the maximum horizontal stress is regionally oriented 138°N (Fig. 14). Vertical stress derived from density, checkshot and sonic log data ranges from 20 MPa at 1 km depth to 66 MPa at 3 km depth (slightly less than 1 psi/ft; Fig. 14). Analysis of 8 leak-off tests conducted in the Gippsland Basin indicates the minimum horizontal stress magnitude is close to S_v (~20.5 MPa/km; Fig. 14). The magnitude of $S_{h\,min}$ cannot be determined absolutely in stress environments where horizontal fractures form at the wellbore wall. This is because the fracture opens against S_v. The presence of TDITFs suggest that it is possible that leak-off tests form horizontal fractures in West Tuna. However, the leak-off test pressures are still critical to in situ stress determination and establish that $S_{h\ min} \geqq S_v$ (border of strike-slip and reverse faulting) in West Tuna. Modular Dynamic Test data in West Tuna suggests hydrostatic pore pressure at the depth of interest (above 2800 m; Fig. 14). These data can be combined with the observations of transverse DITFs to constrain $S_{H\,max}$.

4.1. Constraining $S_{H\,max}$ magnitude

The transverse DITFs observed in the West Tuna image logs were observed in the cemented units of the R- and S-reservoirs. Rock strength testing of similar units in the Gippsland Basin indicates that $\mu \sim 0.65$ and $\nu \sim 0.28$. The allowable stress regime in Fig. 15 is based on $\mu \sim 0.65$. Since transverse DITFs were observed in West Tuna, Eqs. (18) and (20) may be plotted as lines on the allowable region diagram to determine the stress region in which transverse DITFs may form (Fig. 15). Considering the criterion that $\sigma_{\theta\theta} \geqslant \sigma_{zz}$ (Eq. (20)) and the known parameters of the in situ stress tensor (S_v~21 MPa/km, P_p~9.8 MPa/km and P_w~9.8 MPa/km), the allowable values for $S_{H\,max}$ must lie in the

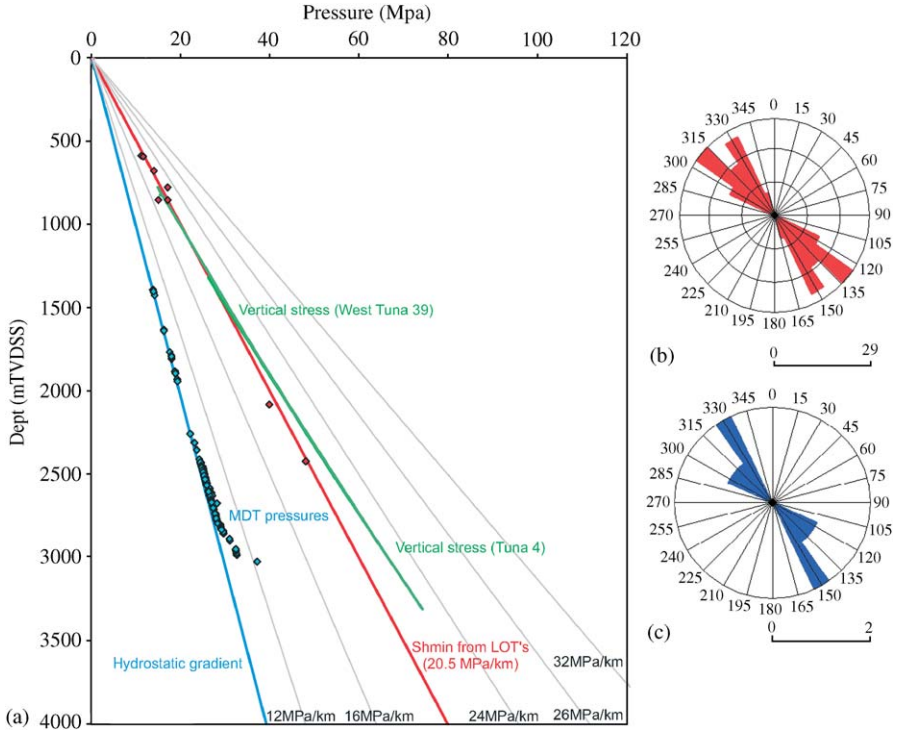

Fig. 14. (a) In situ stress tensor for the West Tuna area. MDT pressures indicate that pore pressure is hydrostatic above ~2800 m. Vertical stress was derived from density and checkshot data in two wells (Tuna_4 and West Tuna_39). The gradient is consistent and 20 MPa at 1 km depth and 66 MPa at 3 km depth. Eight leak-off tests suggest that the $S_{h\,min}$ is ~20.5 MPa/km which is close to S_v particularly at shallow depths. (b) $S_{H\,max}$ orientation from 96 breakouts on image logs from 6 West Tuna wells. (c) $S_{H\,max}$ orientation from 4 DITFs on image logs from 6 West Tuna wells.

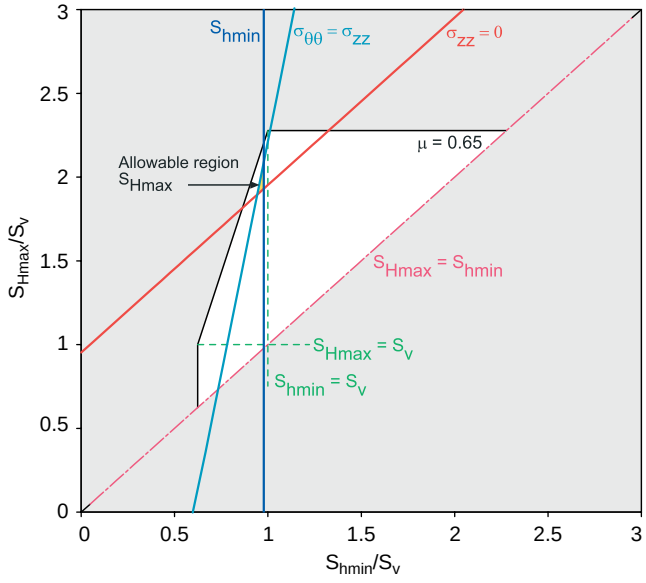

Fig. 15. Allowable values of $S_{H\,max}$ constrained by the occurrence of transverse DITFs in West Tuna. If $S_{h\,min}$ derived from leak-off tests is considered an upper bound to $S_{h\,min}$ then the allowable values of $S_{H\,max}$ in West Tuna lie in the shaded area marked.

region to the right of the line representing $S_{qq} = S_{zz}$ in Fig. 15. Similarly the criterion $\sigma_{zz} \leqslant 0$ (Eq. 18) constrains the allowable values of $S_{H\,max}$ to the line representing $S_{zz} = 0$ in Fig. 15. The observation of transverse DITFs in the West Tuna area constrains the stress field to one on the border of strike-slip and reverse faulting ($S_{H\,max} \gg S_{h\,min} \sim S_v$), without requiring prior knowledge of $S_{h\,min}$ or $S_{H\,max}$.

It is reassuring to note that the high $S_{h\,min}$ required (theoretically) for transverse DITFs to develop (close to or greater than S_v) is consistent with the estimate of $S_{h\,min}$ from leak-off tests in West Tuna (~20.5 MPa/km). If the upper bound to $S_{h\,min}$ is plotted on the allowable region diagram then $S_{H\,max}$ can be constrained to the shaded area in Fig. 15. Substitution of $S_{h\,min} = 20.5$ MPa/km into Eq. (18) and (20) limits the $S_{H\,max}$ magnitude in West Tuna to between 40.5 and 43.7 MPa/km (or $S_{H\,max}/S_v$~1.9–2.1, respectively).

5. Conclusions

Elastic theory not only predicts the formation of transverse DITFs but also suggests that they can only develop in a restricted set of stress states and are diagnostic of the relative in situ stress magnitudes ($S_v \sim S_{h\,min} < S_{H\,max}$). Features that are horizontal across a vertical wellbore are traditionally not picked on image logs because they are difficult to confidently distinguish from bedding. However, the mathematical criterion for transverse DITFs has been used to formulate the following guidelines for interpretation of transverse DITFs on image logs.

Transverse DITFs must be:

- transverse across the wellbore;
- electrically conductive;
- discrete and confined to the tensile region of the wellbore;
- non planar (they show small kinks and are not perfectly straight); and
- discordant to bedding.

Fractures meeting the criterion described above were observed in image logs from the West Tuna area of the Gippsland Basin and the fractures have been interpreted as drilling-induced. Furthermore, the high value of $S_{h\,min}$ required for transverse DITFs to develop (close to or greater than S_v) is consistent with the estimate of $S_{h\,min}$ from leak-off tests in West Tuna.

The occurrence of transverse DITFs allows the stress regime to be constrained to the border of a strike-slip and reverse faulting regime without requiring knowledge of $S_{h\,min}$ ($S_{h\,min} \sim S_v$, and $S_{H\,max}$~twice $S_{h\,min}$). Since $S_{h\,min}$ could be estimated from leak-off tests, the magnitude of $S_{H\,max}$ in the West Tuna area can be constrained to ~40–44 MPa/km.

References

[1] Zoback MD, et al. Determination of stress orientation and magnitude in deep wells. Int J Rock Mech Min Sci 2003;40:1049–76.
[2] Bell JS, Gough DI. Northeast-southwest compressive stress in Alberta—evidence from oil wells. Earth planet Sci Lett 1979;45:475–82.
[3] Brudy M, Zoback MD. Drilling-induced tensile wall-fractures: implications for determination of in situ stress orientations and magnitudes. Int J Rock Mech Min Sci 1999;36:191–215.
[4] Peska P, Zoback MD. Compressive and tensile failure of inclined wellbores and determination of in situ stress and rock strength. J Geophys Res 1995;100(B7):12791–811.
[5] Bell JS. In situ stresses in sedimentary rocks (part 1): measurement techniques. Geoscience Canada 1996;23(2):85–100.
[6] Wiprut D, et al. Compressive and tensile failure of inclined well bores and determination of in situ stress and rock strength. J Geophys Res 1997;100:1279–81.
[7] Barton CA, et al. Characterising the full stress tensor based on observations of drilling-induced wellbore failures in vertical and inclined boreholes leading to improved wellbore stability and permeability prediction. APPEA J 1998;38(1):466–87.
[8] Brudy M, Kjorholt H. Stress orientation on the Norwegian continental shelf derived from borehole failures observed in high-resolution borehole imaging logs. Tectonophysics 2001;337:65–84.
[9] Morin R, Flamand R. Analysis of stress-induced oval features in a borehole at Deep Sea Drilling Project Site 504, eastern equatorial Pacific. J Geophys Res 1999;104(B2):2767–75.
[10] Aadnoy BS. Inversion technique to determine the in situ stress field from fracturing data. J Petrol Sci Eng 1990;4:127–41.
[11] Amadei B, Stephansson O. Rock stress and its measurement. London: Chapman & Hall; 1997.

[12] Jaeger JC, Cook NGW. Fundamentals of rock mechanics. 3rd ed. London, United Kingdom: Chapman & Hall; 1979.
[13] Kirsch G. Die Theorie der Elastizitat und die Beaurforisse der Festigkeitslehre. Z Ver Deut Ingen 1898;42:797–807.
[14] Moos D, Zoback MD. Utilization of observations of wellbore failure to constrain the orientation and magnitude of crustal stresses: application to continental, deep sea drilling project and ocean drilling program boreholes. J Geophys Res 1990;95(B6):9305–25.
[15] Haimson B, Fairhurst C. Initiation and extension of hydraulic fractures in rocks. Soc Petr Eng J 1967:310–8.
[16] Sibson RH. Frictional constraints on thrust, wrench and normal faults. Nature 1974;249:542–4.
[17] Handin J. On the Coulomb–Mohr failure criterion. J Geophys Res 1969;74(22):5343–8.
[18] Anderson EM. The dynamics of faulting and dike formation with application in Britian. 2nd ed. Edinburgh: Oliver and Boyd; 1951.
[19] Barton CA. Discrimination of natural fractures from drilling-induced wellbore failures in wellbore image data—Implications for reservoir permeability. In: SPE International Petroleum Conference and Exhibition: Villahermosa; 2000.
[20] Berard T, Cornet FH. Evidence of thermally induced borehole elongation: a case study at Soultz, France. Int J Rock Mech Min Sci 2003;40:1121–40.
[21] Prensky S. Borehole breakouts and in situ rock stress—a review. The Log Analyst 1992;33:304–12.
[22] Bell JS. Petro Geoscience 1. In situ stresses in sedimentary rocks (part 1): measurement techniques. Geoscience Canada 1996;23(2):85–100.
[23] Bell JS. Practical methods for estimating in situ stresses for borehole stability applications in sedimentary basins. J Petrol Sci Eng 2003;38(3–4):111–9.
[24] Tingay MRP, et al. Variation in vertical stress in the Baram Basin, Brunei: Tectonic and geomechanical implications. Mar Petrol Geol 2003;20(10):1201–12.
[25] Breckels IM, van Eekelen HAM. Relationship between horizontal stress and depth in sedimentary basins. J Petrol Technol 1982;34:2191–8.
[26] Aadnoy BS, Chenevert ME. Stability of highly inclined boreholes. SPE Drilling Eng 1987;2:364–74.
[27] Goode PA, Pop JJ, Murphy WF. Multiple-probe formation testing and vertical reservoir continuity. Soc Petrol Eng J 1991;SPE 22738:787–96.
[28] Zimmerman T, et al. Application of emerging wireline formation testing technologies. In: Eighth Offshore South East Asia Conference. Singapore: OSEA 90105; 1990.